01

Experimental study of Doppler effect impact on isotopically selective photoionization of lutetium

© A.B. D'yachkov, A.A. Gorkunov, S.K. Kovalevich, A.V. Labozin, S.M. Mironov, V.A. Firsov, G.O. Tsvetkov, V.Ya. Panchenko

National Research Center „Kurchatov Institute“,
Moscow, Russia

e-mail: Tsvetkov_GO@nrcki.ru

Received June 25, 2025
Revised November 20, 2025
Accepted December 01, 2025

The impact of the Doppler effect on isotopically selective laser photoionization of lutetium has been experimentally studied using a three-step scheme $5d6s^2\,{}^2D_{3/2}-5d6s6p\,{}^4F^o_{5/2}-5d6s7s\,{}^4D_{3/2}-(53375\,\mathrm{cm}^{-1})^o_{1/2}$.

Keywords: laser isotope separation, laser selective photoionization, lutetium-177.

DOI: 10.61011/EOS.2025.12.63187.8323-25

Introduction

The method of laser photoionization isotope separation in an atomic vapor (AVLIS method) used for separation of lutetium isotopes is quite promising both, in terms of extracting the isotope ^{176}Lu (natural content of 2.49 %) from the natural mixture, and obtaining the radionuclides ^{177}Lu and ^{177m}Lu from lutetium that has been irradiated with neutrons in a reactor. These processes can be used to produce the radionuclide of ^{177}Lu for its medical application [1,2].

The laser photoionization method provides for the flow of atoms of the initial substance to be directed into a working volume filled with laser radiation where the selective photoionization of atoms of the target isotope occurs. The obtained photoions of the target isotope are pulled out by electric field to the product collector, while the atoms of other isotopes, remaining neutral, continue their way along a straight line to the waste collector.

When designing the working volume in the laser photoionization method, one of the key parameters is the angle of divergence of the atomic flow. This parameter determines the properties of an ensemble of atoms interacting with laser radiation, since atoms flying at different angles to the laser beam due to the Doppler effect perceive laser radiation somewhat shifted towards a higher or lower frequency. To make a reasonable choice of the divergence angle, it is necessary to know how the laser radiation tuning consistent with the atom deflection affects the selectivity and efficiency of photoionization. This paper outlines an experimental study of the impact of Doppler effect on the selectivity and efficiency of lutetium photoionization with respect to the problem of extracting ^{176}Lu isotope from a natural mixture.

Since isotopes of the natural mixture of ^{175}Lu and ^{176}Lu have nonzero nuclear spin, all energy levels are split into multiplets (see Fig. 1, 2). The sublevels in the multiplets are determined by the total atomic moment $F = J + I, J + I - 1, \ldots, |J - I|$, where J —is the total electron moment of the atom, I —is the spin of the nucleus. The spectrum of the hyperfine structure (HFS) consists of transitions between the multiplets sublevels with a change in moment $\Delta F = 0, \pm 1$, as a result of which the optical spectrum of photoionization for each isotope consists of 30 lines. The lines frequency difference, as a rule, significantly exceeds the spectral width of the laser radiation. Thus, with a certain laser setting, photoionization is carried out only along one chain of lines of the first, second and third stages —the photoionization channel. The number of possible channels, allowing for the selection rules, reaches 44.

Selective photoionization using a three-stage scheme $5d6s^2\,{}^2D_{3/2}-5d6s6p\,{}^4F^o_{5/2}-5d6s7s\,{}^4D_{3/2}-(53375\,\mathrm{cm}^{-1})^o_{1/2}$ was studied in theoretical work [3,4]; the findings from [4] were the closest to experimental ones, however, these results were obtained using mixed-polarization lasers, while in our experiments we always used laser radiation with linear polarization, and the direction of the laser radiation polarizations of all three stages coincided. The correctness of this choice is proved by the results of experiment [5], where photoionization was studied using the most efficient channels with different laser radiation polarizations. The experimental results are well in line with the theory if the atoms interaction with laser radiation is assumed to be coherent, characterized by a Rabi frequency, and combinations of individual projections M of the atom's total mechanical moment F of transitions are expected to behave like closed systems. Then, in case of linear polarization, the selection rule $\Delta M = 0$ results in the ratio of the dipole moments of the first and second transitions staying the same for all projections, and it is now possible to choose the ratio of laser radiation intensities, which ensures equality of Rabi frequencies at

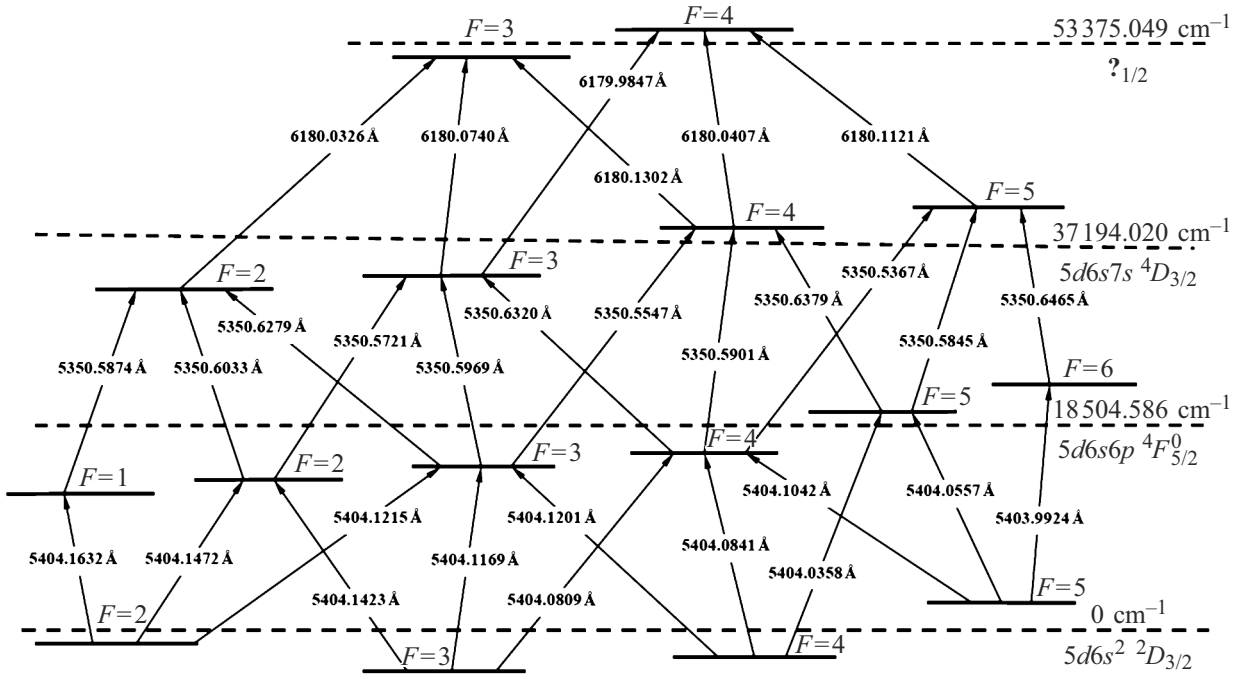

Figure 1. Photoionization scheme for ^{175}Lu isotope ($I = 7/2$). Wavelengths for vacuum.

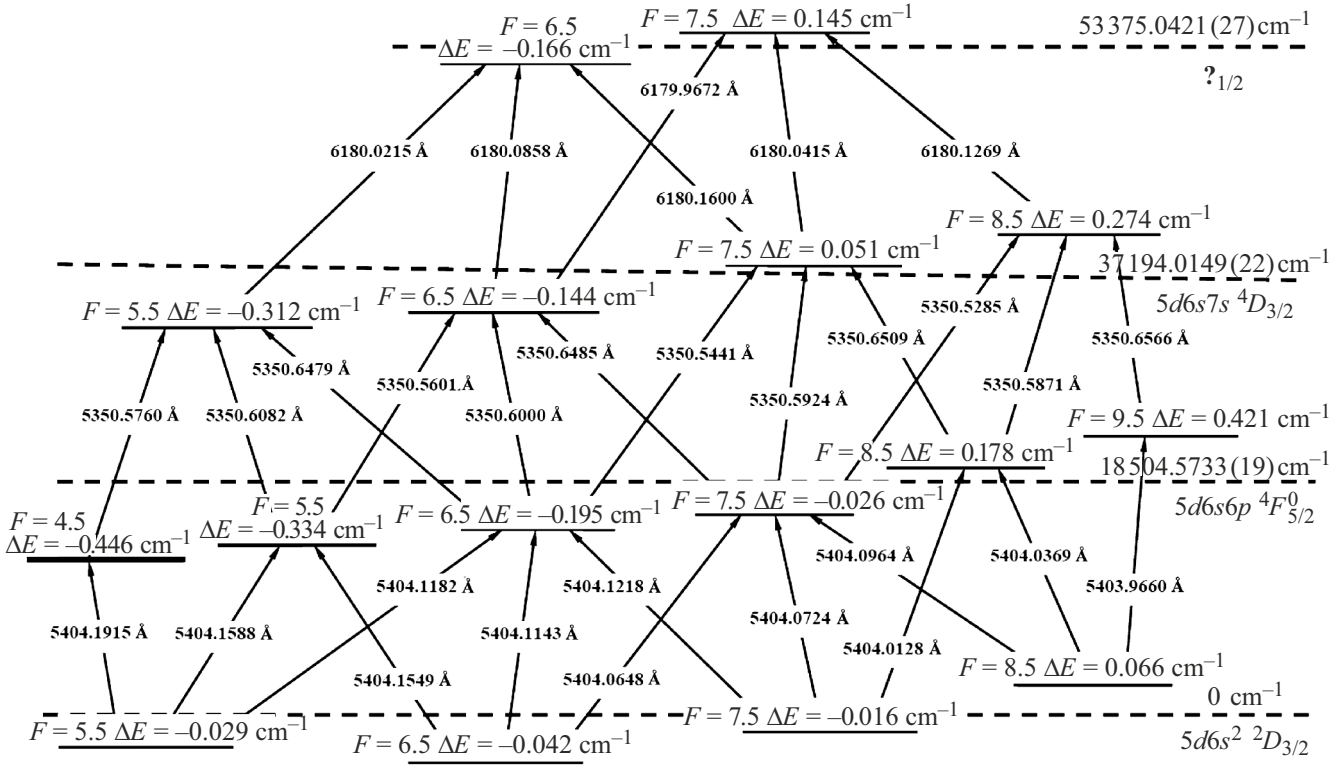

Figure 2. Photoionization scheme for ^{176}Lu isotope ($I = 7$). Wavelengths for vacuum.

the first and second transitions for all combinations of projections obeying the selection rule $\Delta M = 0$. In case of circular polarization, the selection rule $\Delta M = \pm 1$ and the ratio of the dipole moment of the first and second transitions turn out to be different for different combinations of projections. Because of this, when selecting the laser radiation intensities, the equality of the Rabi frequencies of the first and second transitions may be ensured only for a

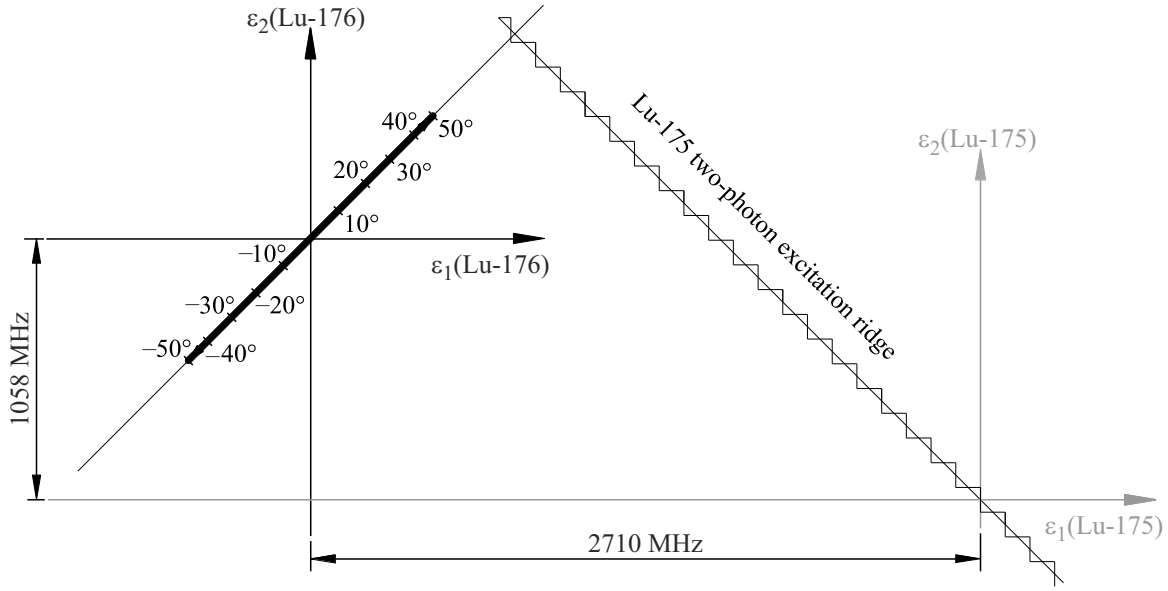

Figure 3. The line (solid line) of variation of the laser radiation frequency versus resonance of the first and second transitions at various flight angles of atoms of the target, ^{176}Lu, and non-target, ^{175}Lu isotopes in the working volume.

small number of projection combinations, while for other combinations, the Rabi frequencies at the first and second transitions will be very different and photoionization will be ineffective.

The most efficient and selective channel of ^{176}Lu isotope photoionization is channel 8.5−9.5−8.5−7.5 [4], since as an initial component it uses the most occupied component of the ground state from $F = 8.5$ (occupancy 0.3), and also since the transition lines are the most distant from the corresponding lines of the non-target ^{175}Lu isotope at the frequency scale. In case of selective photoionization of lutetium ^{176}Lu isotope in channel 8.5−9.5−8.5−7.5 the closest and most probable photoionization channel of the non-target ^{175}Lu isotope is channel 5−6−5−4. The difference between the frequencies of the corresponding resonances is −2710 MHz at the first transition, and +1058 MHz at the second transition. Fig. 3 illustrates the scheme of changing the tuning of frequencies ε_1 and ε_2 on the resonances of the first and second transitions, respectively, for ^{175}Lu and ^{176}Lu isotopes. It can be seen from the figure that the resonance point of the target isotope ^{176}Lu is located in the sector formed by the resonance axis along the second transition (axis $\varepsilon_2 = 0$ for ^{175}Lu) and the crest of the two-photon transition ($\varepsilon_1 = -\varepsilon_2$) of the non-target isotope ^{175}Lu (Fig. 3). For the positive angles of atomic flight, the angles at which the detuning corresponds to an approximation to the two-photon ridge of the non-target ^{175}Lu isotope are selected, respectively, at negative angles, the approach to the resonance axis occurs along the second transition of the non-target ^{175}Lu isotope. Thus, when atoms deviate from the vertical in any direction (both towards the laser beam and along the laser beam), conditions arise for increasing photoionization of the non-target ^{175}Lu isotope.

In the experimental study of Doppler effect using a narrow atomic beam intersecting with laser beams at an angle of 90°, the laser radiation wavelengths of all three stages of a three-stage lutetium photoionization scheme are adjusted so that the laser radiation frequencies perceived by an atom correspond to those perceived by an atom flying at an angle γ to the laser radiation flow. An atom flying along (or towards) a laser beam at a speed of v perceives the frequency of the laser field ν

$$\nu = \frac{c - v}{\lambda} = \frac{c(1 - v/c)}{\lambda} = \nu_0\left(1 - \frac{v}{c}\right), \qquad (1)$$

where ν_0 — true frequency of laser radiation, c — velocity of light.

An atom with a speed of V at some angle γ to an axis perpendicular to the direction of the beam has a velocity projection onto the direction of the beam

$$v = V \sin\gamma. \qquad (2)$$

Thus, the frequency of the laser field for this atom will be

$$\nu = \nu_0\left(1 - \frac{V \sin\gamma}{c}\right), \qquad (3)$$

and the wavelength, respectively

$$\lambda = \frac{c}{\nu} = \frac{c}{\nu_0(1 - \frac{V \sin\gamma}{c})} = \frac{\lambda_0}{(1 - \frac{V \sin\gamma}{c})}. \qquad (4)$$

Thus, an atom flying perpendicular to the laser beam interacts with laser radiation with a wavelength of λ as an atom flying at an angle of γ to an axis perpendicular to the

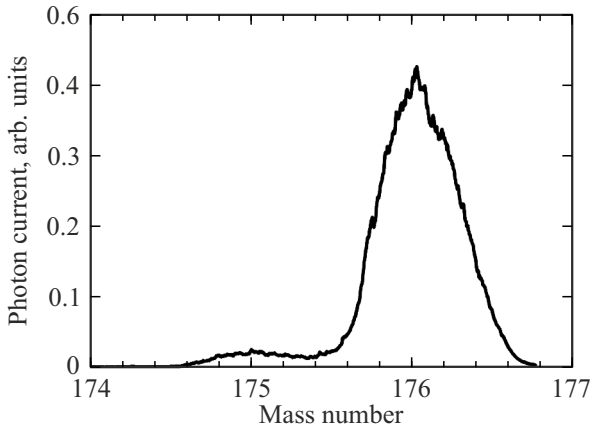

Figure 4. The mass spectrum of the photoionic current at wavelengths corresponding to the angle $+15°$ and the average power density at the first, second, and third stages 68 mW/cm^2, 26 mW/cm^2 and 2.25 W/cm^2 respectively.

Table 1. Wavelengths of the first, second, and third stages of photoionization of ^{176}Lu isotope along the 8.5−9.5−8.5−7.5channel versus angle γ at an average velocity of 492 m/s (evaporation temperature 1700 K)

Angle γ	Wavelength, Å		
	first stage	second stage	third stage
−30°	5403.9616	5350.6522	6180.1218
−25°	5403.9623	5350.6529	6180.1226
−20°	5403.9630	5350.6536	6180.1234
−15°	5403.9637	5350.6543	6180.1243
−10°	5403.9645	5350.6551	6180.1251
−5°	5403.9652	5350.6558	6180.1260
0	5403.9660	5350.6566	6180.1269
5°	5403.9668	5350.6574	6180.1278
10°	5403.9675	5350.6581	6180.1287
15°	5403.9683	5350.6589	6180.1295
20°	5403.9690	5350.6596	6180.1304
25°	5403.9697	5350.6603	6180.1312
30°	5403.9704	5350.6610	6180.1320

beam direction would interact with laser radiation with a wavelength of λ_0. Based on the formula (4) the wavelengths were summarized in Table 1 to study the photoionization of ^{176}Lu isotope for the average velocity of lutetium atoms 492 m/s, which is realized at an evaporation temperature of 1700 K.

It should be noted that when lutetium evaporates, the temperature is 1700−2300 K. When using a temperature greater than 1700 K, the speed of the atom increases, however, the sets of wavelengths from Table 1 will still reflect the sets of frequencies perceived by the atom, but at smaller angles. Thus, the deflection angle 30° at a temperature of 1700 K (average velocity of atom $\sim$ 490 m/s) corresponds to the angle 27.4° at a temperature of 2000 K (average velocity of atom $\sim$ 530 m/s) and angle 25.5° at a temperature of 2300 K (average velocity of atom $\sim$ 570 m/s).

Experiment

The experiment was carried out in a vacuum chamber equipped with a metallic lutetium vaporizer and a quadrupole mass spectrometer MS-7302. An atomic beam with a full divergence angle of 0.2° (Doppler broadening 10 MHz) intersected with a laser beam at a right angle in the ionization chamber of the ion source of the mass spectrometer. The interaction area represents a 2 mm diameter 2 mm long cylinder. The photoions are pulled out by the ion optical system of the mass spectrometer and registered using a secondary electron multiplier. This makes it possible to determine the value and isotopic composition of the photoionic current. Radiation produced by three pulsed single-mode dye lasers (DLs) pumped by copper vapor lasers was used tor resonance excitation and ionization of atoms. The spectral width of DLs lasing line was 100−150 MHz (FWHM), the pulse duration (FWHM) was 20 ns, the pulse repetition rate was 10 kHz, and the emission of all three lasers was polarized linearly in the same direction. The laser pulses of the first, second and third stages were combined in time. The technical parameters and features of the experimental setup were characterized in detail in [6,7]. In the experiment, the laser wavelengths were adjusted according to the values in Table. 1 at a certain angle, and the mass spectrum of the photoionic current was recorded.

The study was conducted for two sets of laser radiation intensity. The first set corresponds to the average power densities of 35 mW/cm^2, 22 mW/cm^2 and 2.25 W/cm^2 (average intensities allowing for the ratio of pulse repetition duration and frequency, 175 W/cm^2, 110 W/cm^2 and 11.25 kW/cm^2) at the first, second and third photoionization stages, which is approximately equal to the laser radiation parameters used in [8], where, as a result of direct measurement, the degree of photoionization extraction of ^{175}Lu isotope from the atomic flux 0.17 was obtained. Taking into account that the occupancy of the ground state of lutetium at the evaporation temperature is 0.7, and the occupancy of HFS sublevel is 0.34, the maximum possible degree of extraction is 0.24, and the degree of extraction experimentally obtained in [8] using a narrow atomic beam 0.17 corresponds to the probability of photoionization of atoms during passage the irradiated volume is 0.7. Thus, the combination of laser radiation intensities used in this study conforms to the saturation approximation and can be used in industrial photoionization for lutetium extraction from a narrow atomic beam with a Doppler width of 200−300 MHz. The authors were also interested in expanding the spectral contour of interaction due to field broadening to work with wider atomic fluxes, and therefore the second set differed from the first one in terms of higher intensity, with average power densities at the first,

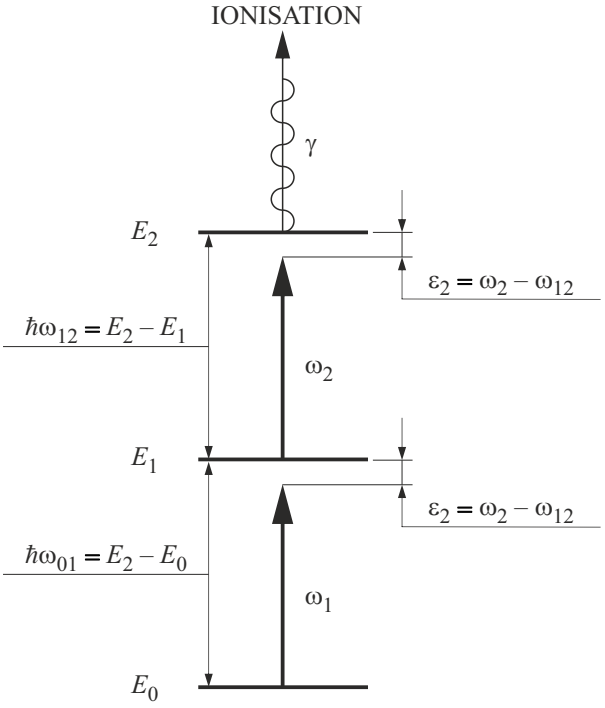

Figure 5. Photo-ionization scheme.

second, and third stages being 68 mw/cm^2, 26 mW/cm^2 and 2.25 W/cm^2 respectively (average intensities 340 W/cm^2, 130 W/cm^2 and 11.25 kW/cm^2).

Table 2 shows the values of the obtained photoionic current of the target isotope ^{176}Lu and its concentration. Fig. 4 illustrates the mass spectrum of the photoionic current at wavelengths corresponding to the angle $+15°$ and the average power density at the first, second, and third stages 68 mW/cm^2, 26 mW/cm^2 and 2.25 W/cm^2 accordingly.

Discussion

It's worth noting the comparison of the obtained results with the analytical assessment. The experience in using narrow-band single-mode lasers shows that multi-stage photoionization is coherent, which is probably due to the fact that a complex of copper vapor lasers with a single master generator is used to pump dye lasers at various stages of photoionization. The coherent nature is evidenced by a decrease in the photoionic signal with the rising intensity of laser radiation of one of the steps above a certain limit, the observation and study of Autler-Townes effect [9,10], as well as the study of the effect of laser radiation polarization on the output of photoions [5]. To describe the coherent interaction, the simplest theoretical approach is to figure out the interaction of monochromatic laser radiation with an atomic system within the time-dependent perturbation theory. When describing a three-level system (Fig. 5) in RWA approximation (rotation wave approximation) a system of three equations is considered [11]:

$$\frac{da_0}{dt} = i\,\frac{1}{2}\,f_1^*\exp(i\varepsilon_1 t)a_1, \tag{5}$$

$$\frac{da_1}{dt} = i\,\frac{1}{2}\,f_1\exp(-i\varepsilon_1 t)a_0 + i\,\frac{1}{2}\,f_2^*\exp(i\varepsilon_2 t)a_2, \tag{6}$$

$$\frac{da_2}{dt} = i\,\frac{1}{2}\,f_2\exp(-i\varepsilon_2 t)a_1, \tag{7}$$

where f_1, f_1^*, f_2 and f_2^* denote the Rabi frequencies of the first and second transitions.

The solution of this system for the upper excited state:

$$a_2(t) = e^{-i\varepsilon_2 t}(C_0 e^{ix_0 t} + C_1 e^{ix_1 t} + C_2 e^{ix_2 t}), \tag{8}$$

where x_0, x_1 and x_2 are the roots of the characteristic equation

$$x^3 + (\varepsilon_1 - \varepsilon_2)x^2 - \left(\varepsilon_1\varepsilon_2 + \frac{f_1^2}{4} + \frac{f_2^2}{4}\right)x + \varepsilon_2\,\frac{f_1^2}{4} - \varepsilon_1\,\frac{f_2^2}{4} = 0, \tag{9}$$

and constants C_0, C_1 and C_2, corresponding to initial conditions

$$a_0(t=0) = 1;\ a_1(t=0) = a_2(t=0) = 0, \tag{10}$$

are equal [12]:

$$C_0 = \frac{f_1 f_2}{4(x_0 - x_1)(x_0 - x_2)}, \tag{11}$$

$$C_1 = \frac{f_1 f_2}{4(x_1 - x_0)(x_1 - x_2)}, \tag{12}$$

$$C_2 = \frac{f_1 f_2}{4(x_2 - x_0)(x_2 - x_1)}. \tag{13}$$

The solution is greatly facilitated by the fact that in laser isotope separation, the laser radiation intensities at the first and second transitions are selected so that the Rabi frequencies at the first and second transitions are the same in order to ensure maximum occupancy of the second excited state and, accordingly, the most effective photoionization of the target isotope. In the experiment in question, the intensities at the first two stages were selected in such a way as to ensure equality of Rabi frequencies as much as possible, although there was a slight excess of intensity at the second stage in the first set. Assuming that the laser radiation is a flat monochromatic wave $E(t) = E_0\cos\omega t$ with linear polarization ($E_0 = \sqrt{8\pi I/c}$), we obtain the expression for the Rabi frequency:

$$f = \frac{|d_{F\grave{F}}|}{\hbar}\sqrt{\frac{8\pi I}{c}}, \tag{14}$$

where $d_{F\grave{F}}$ — projection of the dipole moment vector on direction E_0, I [W/cm^2] — intensity of laser radiation and c [cm/s] — velocity of light. Matrix element of the

Table 2. Experimental results for the target isotope ^{176}Lu

Angle γ	$P_1 = 35\,\mathrm{mW/cm^2}$, $P_2 = 22\,\mathrm{mW/cm^2}$, $P_3 = 2.25\,\mathrm{W/cm^2}$		$P_1 = 68\,\mathrm{mW/cm^2}$, $P_2 = 26\,\mathrm{mW/cm^2}$, $P_3 = 2.25\,\mathrm{W/cm^2}$	
	Signal	Concentration	Signal	Concentration
−30°			0.019	0.74
−25°	0.006	0.76	0.05	0.87
−20°	0.03	0.84	0.15	0.93
−15°	0.10	0.95	0.31	0.91
−10°	0.27	0.98	0.53	0.93
−5°	0.45	0.993	0.66	0.991
0	0.60	0.995	0.75	0.992
5°	0.55	0.990	0.78	0.990
10°	0.43	0.98	0.64	0.97
15°	0.16	0.96	0.42	0.96
20°	0.03	0.92	0.18	0.88
25°	0.007	0.66	0.04	0.73
30°			0.004	0.17

dipole transition moment $d_{F\grave{F}}$ between the states of the hyperfine structure $I, J, F, M \to I, \grave{J}, \grave{F}, \grave{M}$ is expressed via the reduced matrix element $\langle J \parallel D \parallel \grave{J} \rangle$ using formula [13]:

$$d_{F\grave{F}} = (-1)^{F-M} \begin{pmatrix} F & 1 & \grave{F} \\ -M & 0 & \grave{M} \end{pmatrix} (-1)^{I+J+F+1} \times \sqrt{(2F+1)(2\grave{F}+1)} \begin{Bmatrix} J & 1 & \grave{J} \\ \grave{F} & I & F \end{Bmatrix} \langle J \parallel D \parallel \grave{J} \rangle, \quad (15)$$

where F and $\grave{F}$ — quantum numbers of the total mechanic momentum of atom (nucleus and electrons), $\grave{M}$ and M — their projections, $\grave{J}$ and J — quantum numbers of the total angular momentum of electrons, I — nuclear spin. The elements

$$\begin{pmatrix} F & 1 & \grave{F} \\ -M & 0 & \grave{M} \end{pmatrix} \quad \text{and} \quad \begin{Bmatrix} J & 1 & \grave{J} \\ \grave{F} & I & F \end{Bmatrix}$$

represent $3j$- and $6j$- Wigner symbols, respectively [14,15]. Table 3 shows the values of quantum numbers and $6j$ Wigner symbols for the used channel 8.5−9.5−8.5−7.5 for photoionization of the target ^{176}Lu isotope and for the most probable channel 5−6−5−4 for photoionization of the non-target ^{175}Lu isotope. It can be seen from the table that the values of the multipliers are the same for the first and second transitions. When using linearly polarized radiation, transitions between projections with the same value occur: $M = \grave{M}$. $3j$-Wigner symbols for the projections of transitions are given in Table 4 and 5 for the target ^{176}Lu and non-target ^{175}Lu isotopes respectively From the above data, it can be seen that if the laser radiation intensities are chosen so that the Rabi frequencies at the first and second transitions are the same for one projection, then they are the same for all other projections for the target and non-target isotopes. This makes it possible to use one averaged Rabi frequency for all projections and for both isotopes.

In case of equality of frequencies, the Rabi characteristic equation(9) is transformed:

$$x^3 + (\varepsilon_1 - \varepsilon_2)x^2 - \left(\varepsilon_1\varepsilon_2 + \frac{f^2}{2}\right)x + (\varepsilon_2 - \varepsilon_1)\frac{f^2}{4} = 0. \quad (16)$$

Considering the target ^{176}Lu isotope, we assume $\varepsilon_1 = \varepsilon_2 = \varepsilon$ and the roots (11) equal:

$$x_0 = 0,$$
$$x_1 = \sqrt{\varepsilon^2 + \frac{f^2}{2}},$$
$$x_2 = -\sqrt{\varepsilon^2 + \frac{f^2}{2}}. \quad (17)$$

Constants (11)−(13) will be written as

$$C_0 = -\frac{f^2}{4(\varepsilon^2 + \frac{f^2}{2})}, \quad (18)$$

$$C_1 = \frac{f^2}{8(\varepsilon^2 + \frac{f^2}{2})}, \quad (19)$$

$$C_2 = \frac{f^2}{8(\varepsilon^2 + \frac{f^2}{2})}, \quad (20)$$

Probability amplitude of the upper excited state $a_2(t)$

$$a_2(t) = \frac{f^2}{4\left(\varepsilon^2 + \frac{f^2}{2}\right)} \times \left(\frac{e^{i\left(\sqrt{\varepsilon^2+\frac{f^2}{2}}-\varepsilon\right)t} + e^{-i\left(\sqrt{\varepsilon^2+\frac{f^2}{2}}+\varepsilon\right)t}}{2} - e^{-i\varepsilon t}\right), \quad (21)$$

Table 3. Values of quantum numbers and $6j$-Wigner symbols

Quantum number	^{176}Lu		^{175}Lu	
	$^2D_{3/2}-F^o_{5/2}$	$^4F^o_{5/2}-{}^4D_{3/2}$	$^2D_{3/2}-F^o_{5/2}$	$^4F^o_{5/2}-{}^4D_{3/2}$
J	3/2	5/2	3/2	5/2
$\grave{J}$	5/2	3/2	5/2	3/2
F	8.5	9.5	5	6
$\grave{F}$	9.5	8.5	6	5
I	7	7	7/2	7/2
$\begin{Bmatrix} J & 1 & \grave{J} \\ \grave{F} & I & F \end{Bmatrix}$	$-\frac{1}{6}\sqrt{\frac{1}{3}} = 0.096$	$-\frac{1}{6}\sqrt{\frac{1}{3}}$	$\sqrt{\frac{1}{66}} = 0.123$	$\sqrt{\frac{1}{66}}$
$\sqrt{(2F+1)(2\grave{F}+1)}$	$\sqrt{323} = 17.97$	$\sqrt{323}$	$\sqrt{143} = 11.96$	$\sqrt{143}$

Table 4. Absolute values of $3j$-Wigner symbols for transitions in channel 8.5−9.5−8.5 ($^2D_{3/2}-F^o_{5/2}-{}^4D_{3/2}$) of the target ^{176}Lu isotope

$M = \grave{M}$	1/2	3/2	5/2	7/2	9/2	11/2	13/2	15/2	17/2
$\begin{pmatrix} F & 1 & \grave{F} \\ -M & 0 & \grave{M} \end{pmatrix}$	0.162	0.160	0.157	0.151	0.143	0.132	0.118	0.100	0.073

and probability $W_2(t) = |a_2 a_2^*|$ of finding the particle in the upper excited state is equal

$$W_2(t) = \frac{f^4}{16\left(\varepsilon^2 + \frac{f^2}{2}\right)^2}\left(\frac{3}{2} + \frac{1}{2}\cos 2\sqrt{\varepsilon^2 + \frac{f^2}{2}}t - 2\cos\sqrt{\varepsilon^2 + \frac{f^2}{2}}t\right). \quad (22)$$

The time-averaged value of $W_2(t)$ is

$$\overline{W_2(\varepsilon)} = \frac{3}{32}\frac{f^4}{\left(\varepsilon^2 + \frac{f^2}{2}\right)^2}. \quad (23)$$

To evaluate the photoionization of a non-target ^{175}Lu isotope, it is possible at low values of the Rabi frequency:

$$|\varepsilon_1|, \quad |\varepsilon_2| \gg f, \quad (24)$$

to use the approximated roots:

$$x_0 \approx -\varepsilon_1,$$
$$x_1 \approx \frac{\varepsilon_2}{2} + \sqrt{\left(\frac{\varepsilon_2}{2}\right)^2 + \frac{f^2}{2}},$$
$$x_2 \approx \frac{\varepsilon_2}{2} - \sqrt{\left(\frac{\varepsilon_2}{2}\right)^2 + \frac{f^2}{2}}. \quad (25)$$

Accordingly, the constants (11)−(13) will be written as

$$C_0 = \frac{f^2}{4\left(\varepsilon_1^2 + \varepsilon_1\varepsilon_2 - \frac{f^2}{2}\right)}, \quad (26)$$

$$C_1 = \frac{f^2}{8\left(\varepsilon_1 + \frac{\varepsilon_2}{2} + \sqrt{\left(\frac{\varepsilon_2}{2}\right)^2 + \frac{f^2}{2}}\right)\sqrt{\left(\frac{\varepsilon_2}{2}\right)^2 + \frac{f^2}{2}}} = \theta_+, \quad (27)$$

$$C_2 = -\frac{f^2}{8\left(\varepsilon_1 + \frac{\varepsilon_2}{2} - \sqrt{\left(\frac{\varepsilon_2}{2}\right)^2 + \frac{f^2}{2}}\right)\sqrt{\left(\frac{\varepsilon_2}{2}\right)^2 + \frac{f^2}{2}}} = -\theta_-, \quad (28)$$

Probability amplitude of the upper excited state $a_2(t)$

$$a_2(t) = \frac{f^2 e^{-i\left(\varepsilon_1+\varepsilon_2\right)t}}{4\left(\varepsilon_1^2 + \varepsilon_1\varepsilon_2 - \frac{f^2}{2}\right)} + \theta_+ e^{i\left(\frac{\varepsilon_2}{2} + \sqrt{\left(\frac{\varepsilon_2}{2}\right)^2 + \frac{f^2}{2}}\right)t} + \theta_- e^{i\left(\frac{\varepsilon_2}{2} - \sqrt{\left(\frac{\varepsilon_2}{2}\right)^2 + \frac{f^2}{2}}\right)t}. \quad (29)$$

Probability $W_2(t) = |a_2 a_2^*|$ of identifying the particle in the upper excited state is equal

$$W_2(t) = \frac{f^4}{16\left(\varepsilon_1^2 + \varepsilon_1\varepsilon_2 - \frac{f^2}{2}\right)^2} + \theta_+^2 + \theta_-^2 + \theta_+\cos\left(\varepsilon_1 + \frac{\varepsilon_2}{2} + \sqrt{\left(\frac{\varepsilon_2}{2}\right)^2 + \frac{f^2}{2}}\right)t - \theta_-\cos\left(\varepsilon_1 + \frac{\varepsilon_2}{2} - \sqrt{\left(\frac{\varepsilon_2}{2}\right)^2 + \frac{f^2}{2}}\right)t - 2\theta_+\theta_-\cos 2\left(\sqrt{\left(\frac{\varepsilon_2}{2}\right)^2 + \frac{f^2}{2}}\right)t. \quad (30)$$

Table 5. Absolute values of $3j$ Wigner symbols for transitions in channel $5-6-5$ $(^2D_{3/2}-F^o_{5/2}-{}^4D_{3/2})$ of the non-target ^{175}Lu isotope

$M = \grave{M}$	0	1	2	3	4	5
$\begin{pmatrix} F & 1 & \grave{F} \\ -M & 0 & \grave{M} \end{pmatrix}$	0.205	0.202	0.193	0.177	0.153	0.113

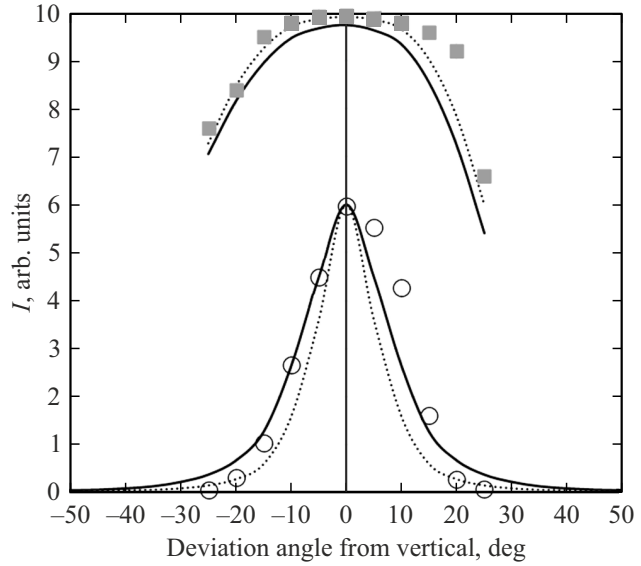

Figure 6. Experimental study of the target isotope ^{176}Lu (circles) signal (relative values) and concentration of ^{176}Lu (squares) versus deflection angle under average power densities at the first, second and third transitions $P_1 = 35\,\text{mW/cm}^2$, $P_2 = 22\,\text{mW/cm}^2$ and $P_3 = 2.25\,\text{W/cm}^2$ respectively. Analysis using Rabi frequency $f = 311$ (solid curves) and 227 MHz (dashed curves).

By averaging $W_2(t)$ in time we get

$$\overline{W_2(\varepsilon_1, \varepsilon_2)} = \frac{f^4}{16\left(\varepsilon_1^2 + \varepsilon_1\varepsilon_2 - \frac{f^2}{2}\right)^2} + \theta_+^2 + \theta_-^2. \qquad (31)$$

It should be noted that the approximate solution of (30) becomes exact when approaching a two-photon ridge ($\varepsilon_1 \sim -\varepsilon_2$) and becomes valid for any ratio of ε and f.

Figure 6 illustrates the experimental and theoretical dependences of the photoionic signal of the target isotope and the concentration of the target isotope in an ensemble of photoions at average power densities at the first, second, and third transitions $P_1 = 35\,\text{mW/cm}^2$, $P_2 = 22\,\text{mW/cm}^2$ and $P_3 = 2.25\,\text{W/cm}^2$ respectively. Figure 7 shows similar results for average power densities at the first, second, and third transitions $P_1 = 68\,\text{mW/cm}^2$, $P_2 = 26\,\text{mW/cm}^2$ and $P_3 = 2.25\,\text{W/cm}^2$ respectively. The theoretical curves for the target isotope signal are obtained by approximating the experimental dependence using formula (23) by the least squares method (solid line). It can be seen that with this approximation, the extreme points corresponding to the

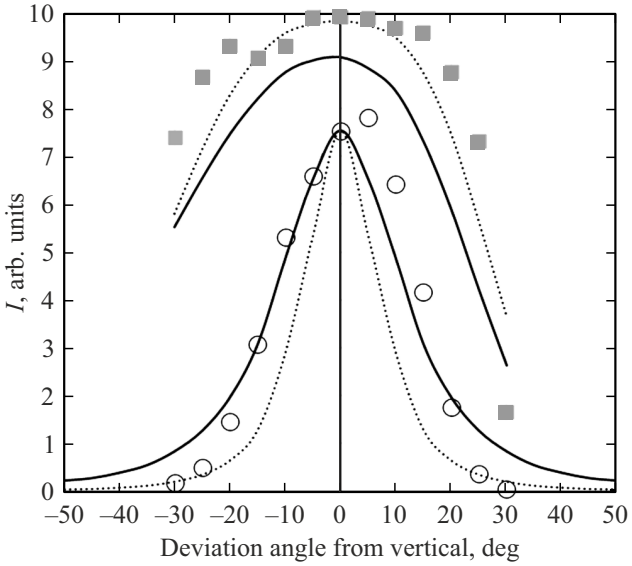

Figure 7. Experimental study of the target isotope ^{176}Lu (circles) signal (relative values) and concentration of ^{176}Lu (squares) versus deflection angle under average power densities at the first, second and third transitions $P_1 = 68\,\text{mW/cm}^2$, $P_2 = 26\,\text{mW/cm}^2$ and $P_3 = 2.25\,\text{W/cm}^2$ respectively. Analysis using Rabi frequency $f = 448$ (solid curves) and 283 MHz (dashed curves).

angles $\pm 20°$, $\pm 25°$ and $\pm 30°$ are significantly lower than the curve. This is explained by the fact that, averaged over a set of pulses, the contour of laser radiation interaction with an ensemble of atoms in the central part depends on the fluctuations in the frequency of laser radiation from pulse to pulse, while during one pulse the contour width is significantly smaller. If we make an approximation using the extreme points (excluding the points $\pm 5°$, $\pm 10°$ and $\pm 15°$), then the obtained value of the Rabi frequency turns out to be noticeably lower, and the concentration curve calculated by the formula

$$C_{176} = \frac{(\overline{W_2(\varepsilon)})_{176} 2.59}{(\overline{W_2(\varepsilon)})_{176} 2.59 + (\overline{W_2(\varepsilon_1, \varepsilon_2)})_{176} 97.41}, \qquad (32)$$

where 2.59 % and 97.41 % — natural concentrations of ^{176}Lu and ^{175}Lu isotopes, accordingly, turn out to be much closer to the experimental values. The fact that the experimental concentration values turn out to be noticeably higher than the estimated ones is explained by that the theoretical model neglects the resonant nature of the third stage of photoionization through the auto ionization state, which increases the experimental selectivity.

The Figures 6 and 7 compared show that there is an increase in the photoionic current of the target isotope with a simultaneous rise in the laser radiation intensity at the first and second stages. This is apparently due to the influence of the spontaneous decay of the second excited state into the first excited state, which in principle cannot be taken into account in the considered theoretical model.

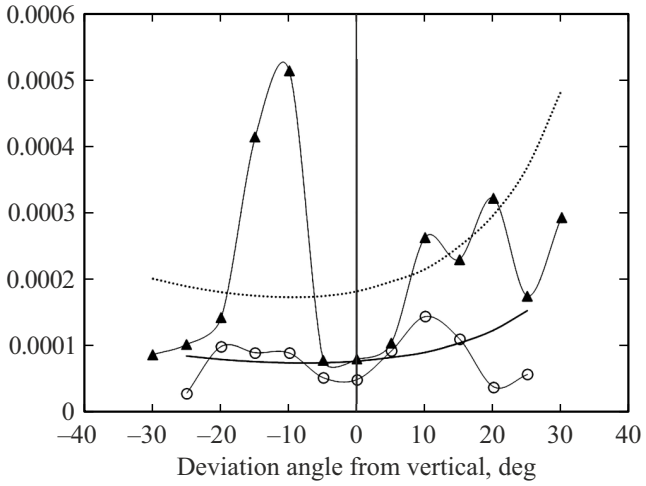

Figure 8. Photoionic current of a non-target isotope versus atomic flow deflection angle at average power densities at the first, second, and third transitions $P_1 = 35\,\text{mW/cm}^2$, $P_2 = 22\,\text{mW/cm}^2$ and $P_3 = 2.25\,\text{W/cm}^2$ respectively (circles) and at $P_1 = 68\,\text{mW/cm}^2$, $P_2 = 26\,\text{mW/cm}^2$ and $P_3 = 2.25\,\text{W/cm}^2$ (triangles). Calculated parameter $(\overline{W_2(\varepsilon_1, \varepsilon_2)})_{175}$ at Rabi frequency $f = 227$ (solid curve) and 283 MHz (dashed curve).

Fig. 8 shows the dependencies of the photocurrent of non-target ^{175}Lu isotope. There is a significant increase in photocurrent at laser wavelength settings corresponding to the angles $-10°$ and $-15°$, which may be caused by the specifics of the dye generators spectrum.

Conclusions

The experimental study sheds light on the degree of decline in efficiency and selectivity of ^{175}Lu isotope photoionization as the deflection angle between the atomic flight line and the perpendicular to the laser beam rises. The data obtained make it possible to determine the integral selectivity and efficiency of photoionization when designing the working volume of the separation unit. Simple analytical estimates based on coherent photoionization of a three-level system are well consistent with the experimental results. Apparently, in mathematical modeling, the most efficient way is to represent laser radiation as a monochromatic one, experiencing stochastic frequency fluctuations from pulse to pulse near the resonant frequency of the target isotope with a normal distribution width of 100−200 MHz. To account for the effect of spontaneous decay of the second excited state into the first excited state, a density matrix apparatus shall be used and it is desirable to calculate the total angular momentum of the atom separately for each combination of projections M . In this case, a three-level system can be considered, and additional selectivity due to resonant photoionization through the auto ionization state can be introduced due to the difference in ionization constants for the target and non-target isotopes. However, taking into account the findings from [10] on the study of Autler-Townes effect of the auto-ionization state, the more interesting is the study of a four-level system experiencing coherent interaction with three-frequency laser radiation, where each frequency independently fluctuates from pulse to pulse around the resonant value.

Funding

This study was carried out under the state assignment of the National Research Center „Kurchatov Institute“.

References

[1] A.B. Dyachkov, A.A. Gorkunov, A.V. Labozina, S.M. Mironov, V.A. Firsov, G.O. Tsvetkov, V.Ya. Panchenko. Physics-Uspekhi, **66** (5), 518–533 (2022). DOI: 10.33367/UFNe.2021.12.039140.
[2] A.B. D'yachkov, A.A. Gorkunov, A.V. Labozina, K.A. Makoveeva, S.M. Mironov, V.A. Firsov, G.O. Tsvetkov, V.Ya. Panchenko. Radiochemistry, **64** (1), 49 (2022). DOI: 10.1134/S1066362222010088.
[3] M.V. Suryanarayana. JOSA B, **38** (2), 353–370 (2021). DOI: 10.1364/JOSAB.409409
[4] Xiaoyong Lu, Lide Wang. Applied Radiation and Isotopes, **210**, 111334 (2024). DOI: 10.1016/j.apradiso.2024.111334
[5] A.B. D'yachkov, A.A. Gorkunov, A.V. Labozin, S.M. Mironov, V.A. Firsov, G.O. Tsvetkov, V.Ya. Panchenko. Opt. Spectrosc., **130** (12), 1525 (2022). DOI: 10.21883/EOS.2022.12.55237.3034-22.
[6] A.B. D'yachkov, A.A. Gorkunov, A.V. Labozin, S.M. Mironov, V.Ya. Panchenko, V.A. Firsov, G.O. Tsvetkov. Quant. Electron., **48** (1), 75 (2018). DOI: 10.1070/QEL16493.
[7] A.B. D'yachkov, A.A.Gorkunov, A.V. Labozin, S.M. Mironov, V.Ya. Panchenko, V.A. Firsov, G.O. Tsvetkov. Instruments Exp. Tech., **61** (4), 548 (2018). DOI: 10.1134/S0020441218040048
[8] A.B. D'yachkov, A.A. Gorkunov, A.V. Labozin, S.M. Mironov, V.Ya. Panchenko, V.A. Firsov, G.O. Tsvetkov. Quant. Electron., **48** (11), 1043 (2018). DOI: 10.1070/QEL16793.
[9] A.B. D'yachkov, A.A. Gorkunov, A.V. Labozin, S.M. Mironov, V.A. Firsov, G.O. Tsvetkov, V.Ya. Panchenko. Quant. Electron., **52** (4), 367 (2018). DOI: 10.1070/QEL18029.
[10] A.B. D'yachkov, A.A. Gorkunov, S.K. Kovalevich, A.V. Labozin, V.A. Firsov, S.V. Fomichev, G.O. Tsvetkov, V.Ya. Panchenko. Opt. Spectrosc., **131** (9), 1119 (2023). DOI: 10.61011/EOS.2023.09.57338.5398-23.
[11] E.M. Lifshitz, L.D. Landau. *Quantum Mechanics; Nonrelativistic Theory* (Pergamon Press, 1965).
[12] I.S. Grigoriev, E.A. Manykin, G.G. Shatalova. *Teoriya trekhstupenchatoi ionizatsii atomov v razryazhennom gaze v lazernom pole* (AEI Report 70/7084, 1996) (in Russian).
[13] B. Shore. Acta Phys. Slovaca. Rev. Tutorials, 58, 243 (2008).
[14] I.I. Sobelman. *Vvedenie v teoriyu atomnykh spektrov* (Fizmatlit, Moscow, 1963) (in Russian).
[15] O. Axner, J.O. Gustafsson, N. Omenetto, J.D. Winefordner. Spectrochim. Acta B, **59**, 1 (2004).

Translated by J.Savelyeva